Molecular Therapy
Methods & Clinical Development
Original Article

Molecular homing and retention of muscle membrane stabilizing copolymers by non-invasive optical imaging in vivo

Addeli Bez Batti Angulski,[1,4] Houda Cohen,[1,4] Mihee Kim,[2,5,4] Dongwoo Hahn,[1] Nicholas Van Zee,[2] Timothy P. Lodge,[2,3] Marc A. Hillmyer,[3] Benjamin J. Hackel,[2] Frank S. Bates,[2] and Joseph M. Metzger[1]

[1]Department of Integrative Biology and Physiology, University of Minnesota Medical School, 6-125 Jackson Hall, 321 Church Street SE, Minneapolis, MN 55455, USA; [2]Department of Chemical Engineering and Materials Science, University of Minnesota, Minneapolis, MN 55455, USA; [3]Department of Chemistry, University of Minnesota, Minneapolis, MN 55455, USA

First-in-class membrane stabilizer Poloxamer 188 (P188) has been shown to confer membrane protection in an extensive range of clinical conditions; however, elements of the systemic distribution and localization of P188 at the organ, tissue, and muscle fiber levels *in vivo* have not yet been elucidated. Here we used non-invasive fluorescence imaging to directly visualize and track the distribution and localization of P188 *in vivo*. The results demonstrated that the Alx647 probe did not alter the fundamental properties of P188 to protect biological membranes. Distribution kinetics in mdx mice demonstrated that Alx647 did not interface with muscle membranes and had fast clearance kinetics. In contrast, the distribution kinetics for P188-Alx647 was significantly slower, indicating a dramatic depot and retention effect of P188. Results further demonstrated the significant retention of P188-Alx647 in the skeletal muscle of mdx mice, showing a significant genotype effect with a higher fluorescence signal in the mdx muscles over BL10 mice. High-resolution optical imaging provided direct evidence of P188 surrounding the sarcolemma of skeletal and cardiac muscle cells. Taken together, these findings provide direct evidence of muscle-disease-dependent molecular homing and retention of synthetic copolymers in striated muscles thereby facilitating advanced studies of copolymer-membrane association in health and disease.

INTRODUCTION

Muscular dystrophies are a diverse group of genetic diseases characterized by progressive muscle deterioration.[1] Among the more devastating muscular dystrophies are those that develop from the absence of components of the dystrophin glycoprotein complex, resulting in compromised sarcolemma integrity in skeletal muscle and heart. One of the most common forms of muscular dystrophy is Duchenne muscular dystrophy (DMD), a fatal disease of progressive muscle deterioration that results from the lack of the cytoskeletal protein dystrophin, which is indispensable for maintaining the structural integrity of the muscle cell membrane.[2]

There is no cure for DMD patients or any effective treatment to prevent or reverse DMD-striated muscle deterioration. There is significant effort in the DMD field focused on gene-based protein replacement strategies to restore dystrophin production, which has shown promise in preclinical studies.[3–6] To date, however, these approaches have not yet been translated successfully in human patients as clinical trials reported recently demonstrate a lack of clinically meaningful success with missed milestones.[7] In this context, it is worth considering additional approaches that target the primary defect of DMD: severe muscle membrane fragility.

As the primary pathophysiological defect in DMD is muscle membrane instability, with subsequent muscle damage and degeneration, a unique therapeutic strategy is the use of synthetic block copolymers as membrane stabilizers to prevent muscle damage by directly stabilizing the dystrophin-deficient muscle membrane.[8] Synthetic block copolymers are a diverse class of soft materials with wide-ranging industrial[9] and biological applications.[10,11] The most studied class of synthetic block copolymers in biomedicine is poloxamers, which are amphiphilic nonionic triblock copolymers composed of a hydrophobic poly(propylene oxide) (PPO) core flanked on both sides by hydrophilic chains of poly(ethylene oxide) (PEO).

In this family of chemicals, the first-in-class membrane stabilizer Poloxamer 188 (P188; 8,400 g mol^{-1}, 80% ethylene oxide content) is the

Received 23 August 2022; accepted 7 December 2022;
https://doi.org/10.1016/j.omtm.2022.12.005.

[4]These authors contributed equally

[5]Present address: Materials Physics and Applications Division, Center for Integrated Nanotechnologies, Los Alamos National Laboratory, NM 87545, USA

Correspondence: Benjamin J. Hackel, Department of Chemical Engineering and Materials Science, University of Minnesota, 356 Amundsun Hall, Minneapolis, MN 55455, USA.
E-mail: hackel@umn.edu
Correspondence: Joseph M. Metzger, Department of Integrative Biology & Physiology, University of Minnesota Medical School, 6-125 Jackson Hall, 321 Church Street SE, Minneapolis, MN 55455, USA.
E-mail: metzgerj@umn.edu

most widely studied copolymer.[12–14] P188 has been found to confer membrane protection against many different types of injuries, including osmotic,[15] oxidative[16] and shear stress,[17] electrical[18] and thermal burns,[11] and other trauma that affects cell membrane integrity.[12,19,20] Membrane stabilization by P188 has also been well established in DMD models where P188 successfully restored muscle cell membrane integrity.[8,21–23] Furthermore, *in vivo* delivery of P188 was shown to prevent myocardial ischemia/reperfusion injury, a leading cause of death in patients with cardiovascular disease, through membrane stabilization.[24–26] These preclinical studies show promise and have led to clinical trials on the use of P188 in human patients to test the safety and efficacy of P188 on endpoints associated with cardiovascular, pulmonary, and musculoskeletal function (ClinicalTrials.gov identifier NCT03558958). Currently, the study is ongoing and no results have yet been reported. Despite wide usage of P188 in preclinical and clinical studies to stabilize membranes from various injury modalities, the distribution and localization of P188 have not yet been fully examined *in vivo*. While the pharmacokinetics, metabolism, and excretion of P188 have been evaluated in humans and animal models,[27,28] little information is available regarding P188 localization and biodistribution for P188 trafficking *in vivo*.

Non-invasive optical imaging provides an excellent approach to investigate the systemic distribution of block copolymers *in vivo*, providing insights into the mechanism of membrane stabilization. However, as P188 itself does not exhibit optical signal properties, it has been challenging to implement a non-invasive optical imaging method to investigate the P188 distribution and localization in animal models. Fluorescent dyes can be tagged to P188, but numerous dyes, especially hydrophobic ones, interact with the cell membrane with the potential to abrogate P188 function.[29] In addition, autofluorescence from biomolecules acting as fluorophores generates background noise in the range of 350–550 nm. Fluorescence probes with absorption and emission wavelengths in the near-infrared (NIR) spectrum (650–900 nm) are most useful for whole-body imaging, as NIR fluorescence dyes are characterized by low cytotoxicity, biocompatibility, and minimum interference from autofluorescence background.[30–32] In addition, NIR dyes provide a convenient and safe method to quantify pharmacokinetics at the subcellular to tissue level while retaining the possibility for quantifying macroscopic organ-level distribution.

The objectives of this study were multifold. First, we focused on the design and implementation of a dye-based method for fluorescence imaging to enable high-fidelity tracking of synthetic copolymer-based membrane stabilizers in striated muscles *in vivo*. Here, Alexa Fluor 647 (Alx647) was implemented because of its relevance for NIR intraoperative imaging as well as its documented minimal interaction with the cell membrane.[29] Second, we tested whether the synthetic triblock copolymer P188 can interact with the sarcolemma of two different cell types (cardiac myocytes and flexor digitorum brevis fibers) *in vitro*. Third, we sought a deeper understanding of the essential elements of the systemic distribution and discrete localization of P188 at the organ, tissue, and muscle fiber levels to enable a comprehensive understanding of the intrinsic physicochemical features of block copolymers guiding muscle membrane association to confer protection *in vivo*. It is currently unclear how P188 localizes to muscle membranes *in vivo*. Accordingly, we implemented a high-resolution non-invasive optical imaging technique to provide the first direct evidence of copolymers surrounding the sarcolemma of skeletal and cardiac muscle cells *in vivo*. Data show direct evidence of P188 surrounding live muscle cells, consistent with P188 membrane stabilization mechanism of action. Most dramatically, live animal imaging shows the preferential homing and retention of copolymers to dystrophin-deficient muscles as compared with dystrophin-replete muscles. We hypothesize that the unique physicochemical architecture and composition of the P188 block copolymer provides the necessary molecule-intrinsic properties to preferentially target damaged muscle membranes *in vivo*.

RESULTS

Copolymer synthesis and characterization

P188-Alx647 was designed based on three considerations: (1) the linker between dye and polymer should be stable in physiological conditions; (2) the fluorescent dye itself should not interact with the cell membrane nor alter the membrane stabilization properties of P188; and (3) the fluorescence excitation and emission wavelengths should fall in the NIR range where tissue autofluorescence is minimal. By these criteria, we developed an amide bond as the linker and Alx647 as the fluorescent dye (λ_{ex} = 651 nm, λ_{em} = 672 nm) (Figures 1A and S1A). For amide bond formation the initial hydroxyl end groups of P188 were converted sequentially to tosyl, azide, and then amine groups (Figures 1A and S1A). Tosylation of hydroxyl end groups of P188 was successful, based on ^{1}H NMR peak appearance at 4.2 ppm (Figure S1B). Peaks at 2.4 ppm, 7.45 ppm, and 7.78 ppm correspond to tosyl ring hydrogens attached to P188 (Figure S1B). Based on peak integration, >95% of hydroxyl end groups were converted to tosyl groups. Substitution of tosyl to azide groups was confirmed, based on the ^{13}C NMR peak at 50 ppm (Figure S1C). No characteristic peaks appeared in the ^{1}H NMR spectrum because the peak for hydrogen next to the azide group (e.g., -CH_2-N_3) overlapped with polypropylene oxide peaks. Reduction of the azide groups to amines was confirmed by the characteristic amine peak at 2.78 ppm. By integrating the area under the peak, we confirmed that ~60% of total end groups were converted to a primary amine. Throughout the reaction, the molecular weight distribution of P188 did not change as evidenced by matrix-assisted laser desorption/ionization time-of-flight (MALDI-TOF mass spectrometry) (Figure 1B). ^{1}H NMR analysis of P188-Alx647 was not possible, as the chemical structure of Alx647 is proprietary. Analysis of the fluorescence intensity of the P188-Alexa647 molecule indicates ~1.7 fluorophores per P188 molecule (Figure S1D). Based on these data, we then used twice as much of Alx647 probe alone as compared with P188-Alx647 as a control for our experiments. By using molar equivalency, we were able to discern that the fluorescent signal obtained from P188-Alx647 was authentic.

To determine whether the protection efficacy of P188 was altered by conjugation with the fluorophore Alx647, a cellular osmotic stress

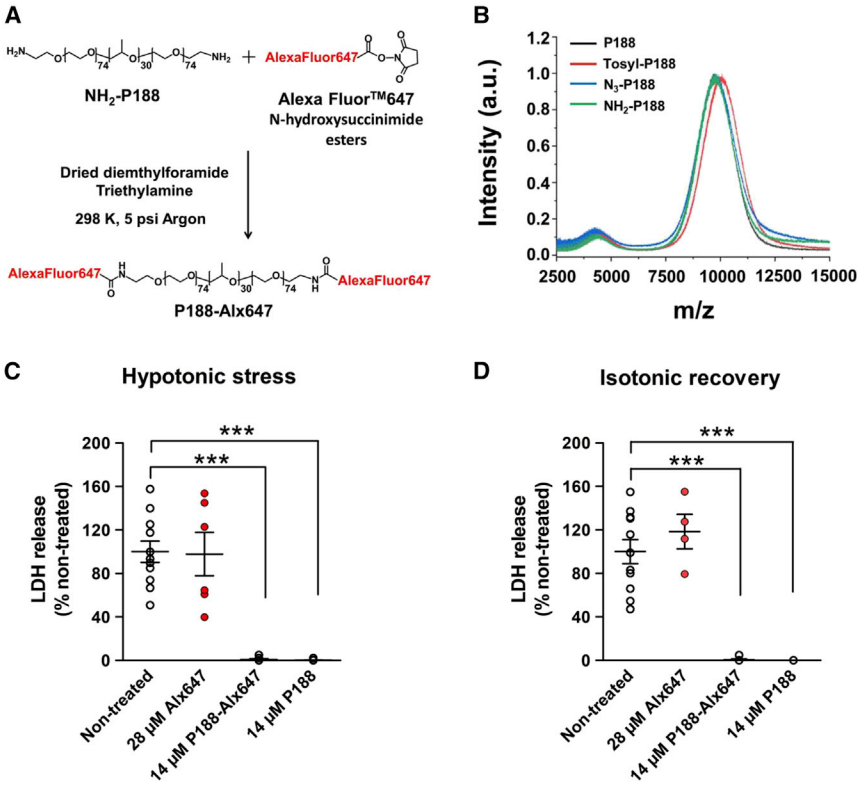

Figure 1. Chemical structure, synthesis, and molecular and cellular characterization of P188-Alx647

(A) Synthesis scheme of P188-Alx647. (B) MALDI-TOF mass spectra of P188, tosyl-P188, N_3-P188, and NH_2-P188. (C and D) P188-Alx647 confers cellular protection not different from P188; 14 μM P188, 14 μM P188-Alx647, or 28 μM Alx647 were added to C2C12 myoblast cultures throughout 134 mOsm hypo-osmotic stress (C) and isotonic recovery (D). LDH release was measured and normalized to non-treated control (buffer only). pH of buffer solution is 7.2. Average ± standard error is shown for 4–6 independent wells per experiment. ***$p < 0.001$.

and lactate dehydrogenase (LDH) tests were employed in a cell-based assay.[15] The LDH release was normalized to the LDH release with buffer solution. Alx647 itself did not protect the cell membrane, as LDH release was similar to that of buffer control (Figures 1C and 1D). Importantly, in the presence of P188-Alx647, LDH release was significantly blunted and not different from P188. Collectively, these results indicate that P188 and P188-Alx647 confer similar protection of the cell membrane and that the Alx647 probe does not affect membrane protection efficacy (Figures 1C and 1D). Thus, overall, we confirmed that this probe did not alter the inherent ability of P188 to interface and protect biological membranes.

Copolymer P188 function *in vitro* and *in vivo*

Previous studies have aimed at understanding the interactions of triblock copolymers with model lipid membranes. These studies have probed the interactions of triblock copolymers with model lipid membranes, such as lipid monolayers at an air-water interface[33] and lipid vesicles.[34–36] However, detailed understanding of the copolymer-lipid interface remains elusive in live cell systems. Thus, we first performed an *in vitro* assay to investigate the P188-membrane interaction using live cardiac myocytes and single flexor digitorum brevis (FDB) fibers isolated from adult animals. Figure 2A (top) shows a confocal micrograph of a representative live cardiac myocyte labeled with calcein (green) and P188-Alx647 (red). The representative image in Figure 2A also highlights the red channel and the black-and-white high-contrast image showing direct evidence of P188 interfacing with the sarcolemma of live single striated muscle cells. Here, P188-Alx647 is visualized decorating the cell membrane surface but not entering the cell. We found similar results when FDB fibers were incubated with P188-Alx647 (Figure 2B). Moreover, our results gain significance by demonstrating similar results between two different species and two different cell types. Unique inherent heterogeneity between muscle cells, including membrane composition and smaller size of cardiac myocytes (~150 μm) relative to FDB fibers (~600 μm), may account for differences in dosage used to label FDB compared with cardiac myocytes. Studies with the Alx647 probe alone show no interaction with the cell membrane (Figures 2A and 2B, bottom). Moreover, we demonstrated P188 located around the cell membrane.

Non-invasive tracking of systemically delivered P188-Alx647 *in vivo*

The next experiments tracked and compared, following subcutaneous systemic delivery, the distribution kinetics of P188-Alx647 and Alx647 in dystrophin-deficient mdx mice and in healthy C57BL/10J (BL10) controls over a 7-day time course (Figure 3A). The results demonstrated that Alx647 alone had fast distribution and fast clearance kinetics, with decay of the fluorescent signal as early as 2 h after the initial subcutaneous injection (Figures 3B–3D). In marked contrast, the kinetics for P188-Alx647 was significantly slower, indicating a dramatic depot and retention effect of P188-Alx647 following systemic injection. The maximum radiance efficiency detected on the ventral view indicates the molecule diffusion peak was reached around 3 h post injection (Figures 3C and 3D) and plateaued for the following few hours before starting a slow decrease over days. At the last experimental time point (day 7), there was a persistent significant systemic fluorescent signal from the mice injected with P188-Alx647. Conversely, the Alx647 signal was not detected after day 1 post injection (Figures 3C and 3D). At the whole-animal level, qualitatively similar distribution kinetics were observed in mdx and healthy BL10 mice (Figures 3 and S2–S4). To the best of our knowledge, this is the first time P188 distribution and localization has been

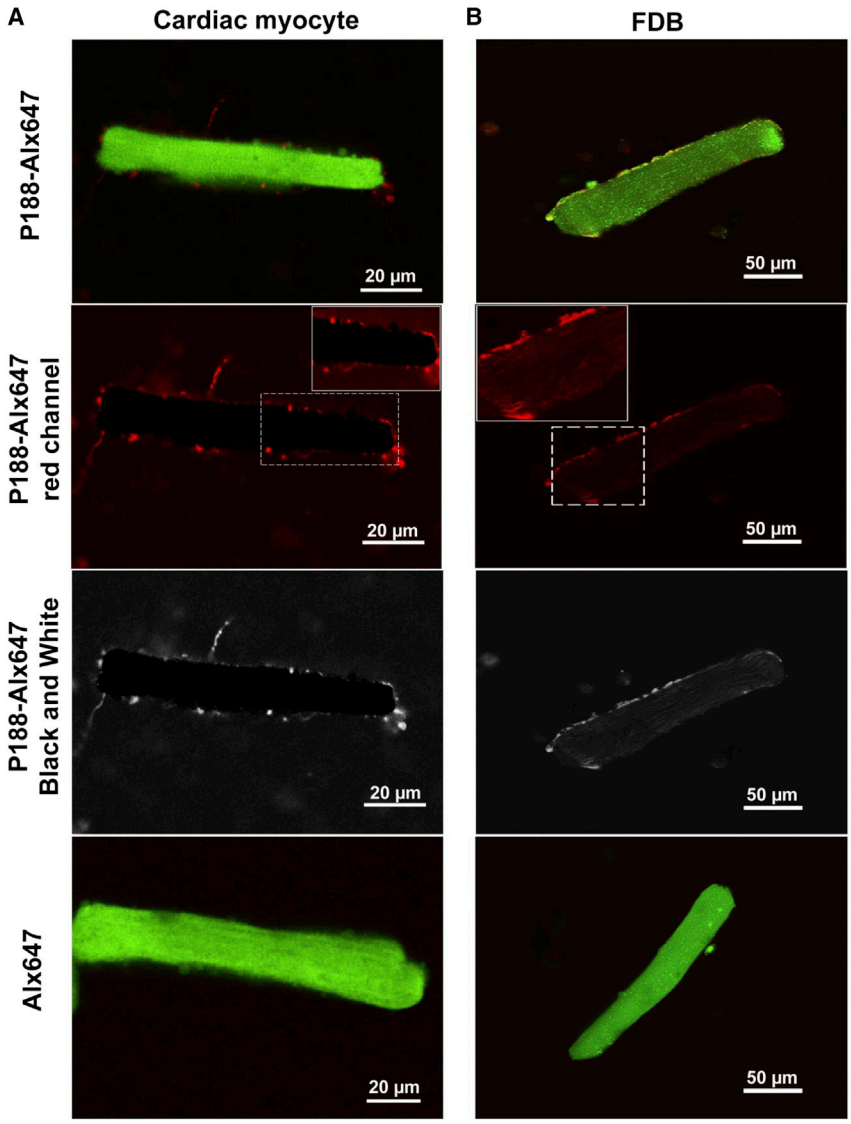

Figure 2. Direct evidence of P188 interfacing with the sarcolemma of live single striated muscle cells

Confocal laser scanning fluorescence microscopy of cardiac myocytes and FDBs following exposure to P188-Alx647. (A) Top: composite image of a rat cardiac myocyte following incubation of 14 μM P188-Alx647 (red). Middle: red channel and black-and-white high-contrast imaging highlights the triblock copolymer 188 surrounding the cardiac myocyte cell membrane. Bottom: a cardiac myocyte following incubation with Calcein-AM (green) and Alx647 (dye only). (B) Top: composite image of a mouse FDB following incubation of 30 μM P188-Alx647 (red). Middle: red channel and black-and-white high-contrast imaging highlights the triblock copolymer 188 surrounding the FDB cell membrane. Bottom: an FDB following incubation with Calcein-AM (green) and Alx647 (dye only). Calcein (green) was used to demonstrate cell viability after incubation with the dye-labeled copolymer P188-Alx647. All these images represent live cell images taken following 4 h incubation with P188-Alx647 or Alx647 at 37°C in FluoroBrite DMEM. Insets show magnifications of boxed regions, with cardiac myocytes and FDB cell membrane highlighted by P188-Alx647. Scale bars represent 20 μm for the cardiac myocyte images and 50 μm for the FDB images. Cardiac myocytes were isolated from female rats aged 3–4 months old, and FDBs were isolated from male mice aged 5–6 months old.

evaluated in the context of skeletal and cardiac muscle using a disease model.

Analysis of the injection site on the dorsal view revealed a persistent high signal from the labeled P188 animal revealing a depot effect following subcutaneous delivery (Figures 3B and S2). Our group previously reported that subcutaneous P188 delivery, but not the intraperitoneal route, conferred significant protection to dystrophic limb skeletal muscle undergoing mechanical stress *in vivo*, showing evidence that a P188 protective effect is critically dependent upon route of delivery.[23] Based on this prior research, we used subcutaneous delivery exclusively in this work. The ability of a single subcutaneous injection to allow a slow continuous release of the copolymer has potential significant clinical implications as related to the administration route, frequency, and adherence to treatment.[37,38]

Distribution of P188-Alx647 in tissues after systemic delivery *in vivo*

After systemic delivery, skeletal muscles, heart, kidney, liver, spleen, and brain were removed to evaluate the organ distribution of P188-Alx647. Interestingly, we found a prolonged retention of the labeled P188 in the skeletal muscle and heart (Figures 4A and 4B). Overall, the tissues harvested from P188-Alx647-injected mice had strong persistent fluorescent signal both at the early (6 h) and late (day 7) timepoints. The results showed an intense fluorescent signal in the kidneys, consistent with reports of non-metabolized P188 elimination.[27,28] The tissues harvested from Alx647-injected mice had a very minimal signal at 6 h with no detectable fluorescent signal at day 7 (Figures 4A and 4B).

P188-Alx647 homing and retention in dystrophin-deficient skeletal muscles *in vivo*

The results demonstrated a prolonged and strong retention of P188-Alx647 in the skeletal muscles of mdx mice (Figure 4). Importantly, comparing the levels of radiance efficiency detected in mdx versus healthy BL10 animals revealed a strong genotype effect in skeletal muscles, in particular triceps, quadriceps, and gastrocnemius, with a significantly higher fluorescence signal in the mdx muscles over dystrophin-replete BL10 mice (Figures 4C–4F and S5). Furthermore, the radiance efficiency levels in kidney, liver, and spleen were significantly

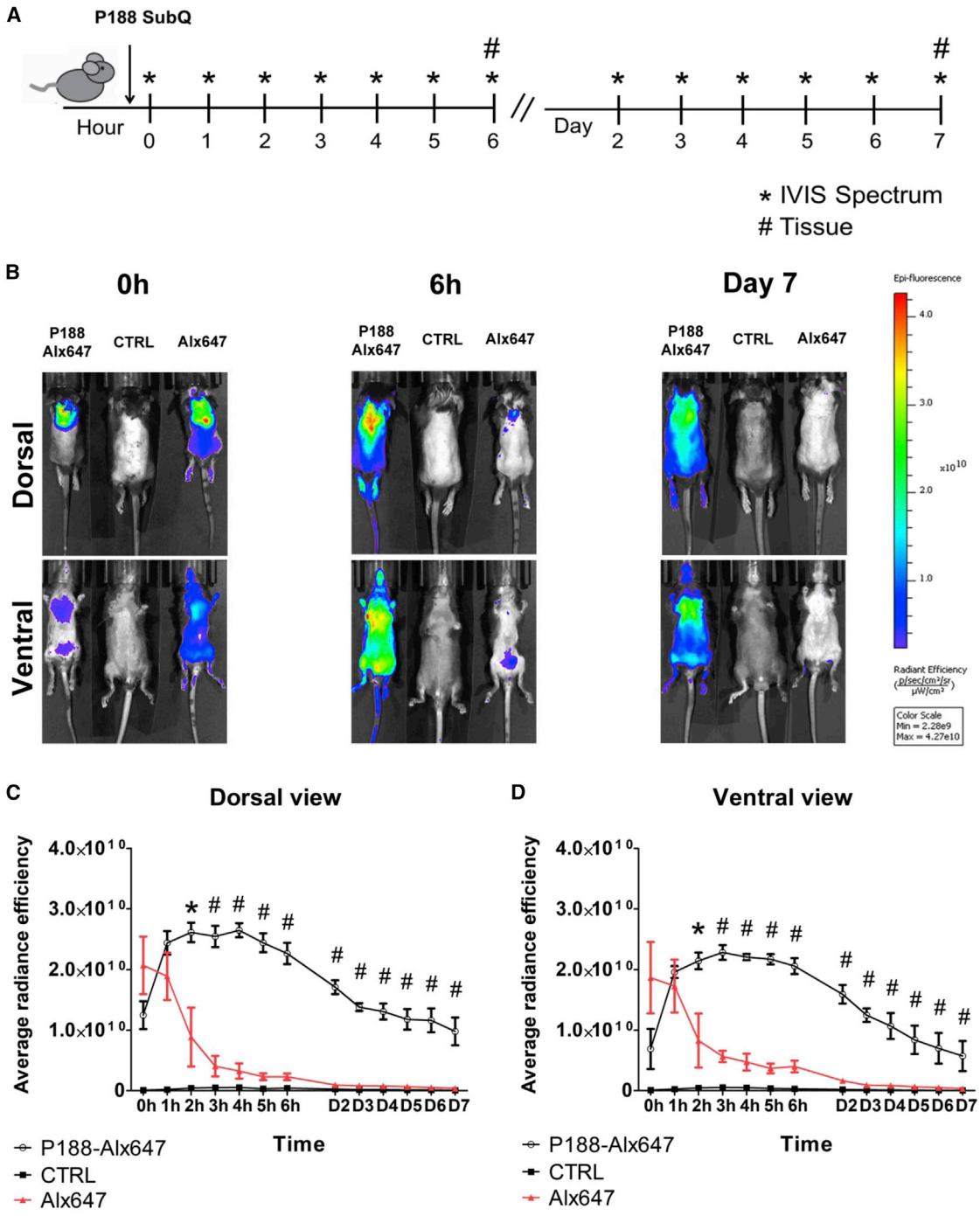

Figure 3. Detection of the systemic distribution of P188-Alx647 in dystrophin-deficient mice *in vivo*

(A) Scheme outlining the design of P188-Alx647 *in vivo* distribution in dystrophin-deficient mice. Young mdx male mice (P21–P25) were injected with a single subcutaneous injection of 150 mg/kg P188-Alx647. The whole-body distribution of P188-Alx647 was assessed by acquiring fluorescence images immediately after the injection (T0 h), followed by 1, 2, 3, 4, 5, and 6 h on day 1 of the experiment and then once a day every 24 h up to day 7. The distribution of P188 was examined by using the IVIS Spectrum live imaging system, providing a qualitative assessment of the whole-body distribution of the triblock copolymer 188 *in vivo*. Asterisks denote the time points where the live images were acquired on the IVIS Spectrum. Hash marks denote the endpoint for tissue collection and further analysis of P188-Alx647 distribution at the organ and tissue level. (B) Overlay of representative grayscale photograph and fluorescent images of a living mdx mouse injected with P188-Alx647. Images of the dorsal (upper) and ventral (lower) planes taken at 0 h, 6 h, and 7 days after injection. A non-injected control mouse is shown in the center, and a mouse injected with Alx647 (dye only) is shown on the right.

(legend continued on next page)

lower in mdx compared with BL10 mice (Figure 4G). These results provide direct evidence of muscle-disease-dependent molecular homing of P188-Alx647, resulting in increased retention of P188-Alx647 in dystrophin-deficient skeletal muscles. We postulate that the membrane instability and skeletal muscle damage secondary to dystrophin loss drives the stronger interaction between P188 and the damaged sarcolemma.

Direct evidence of P188-Alx647 interaction with striated muscles *in vivo*

Next, high-resolution spectral confocal imaging in non-fixed tissues was used to track tissue-level P188 localization upon systemic delivery *in vivo*. The data provide direct evidence of P188-Alx647 surrounding the sarcolemma of skeletal and cardiac muscle cells both at the 6-h (Figure 5) and 7-day timepoints (Figure 6), consistent with the membrane-stabilizing mechanism of action of P188. No signal was detected in tissue samples from mdx mice injected with Alx647, showing no evidence of the dye itself interfacing with the cell membrane (Figure S6A). It is worth noting that the fluorescence imaging protocol was optimized in order to obtain high-quality-resolution images of P188 localization in different muscle tissues. Spectral imaging of each section was performed using fresh/non-fixed cryosections prior to any staining or mounting, to preserve the tissue localization and prevent staining-related modification of the tissue-compound interaction. Linear unmixing of the obtained images using the P188-Alx647 and Alx647 spectra was then performed to separate the specific signal individually and independently of any autofluorescence or artifact. This approach provides direct evidence of the persistence and sarcolemmal localization of P188-Alx647 in the skeletal and cardiac muscles up to a week after a single subcutaneous injection. Subsequent staining with wheat germ agglutinin (WGA), a marker for plasma membrane, further confirmed sarcolemmal interfacing localization of P188-Alx647 in skeletal and cardiac tissue (Figures 7 and S7). These results constitute a live tissue demonstration of conclusions from previous works studying the copolymer-membrane interface performed on lipid bilayers and in atomic model simulations.[36,39]

P188-Alx647 following acute cardiac stress in dystrophic heart *in vivo*

Next, we studied the effect of acute cardiac stress on P188-Alx647 localization in dystrophic mice *in vivo*. The β-adrenergic receptor agonist isoproterenol is commonly used to induce a severe cardiac phenotype in the mdx mouse model, representing an effective model of episodic cardiac injury in dystrophic mice.[40] Isoproterenol is a selective β1/β2-agonist with a strong inotropic and chronotropic effect. The increased workload caused by the rapid increase in heart rate and contractility upon a single isoproterenol bolus leads to contraction-induced membrane damage in the vulnerable cardiac myocytes.[41] In this experiment, mice initially received a subcutaneous injection of P188-Alx647 at 150 mg/kg followed by a single intraperitoneal injection of isoproterenol (10 mg/kg) 4 h after P188 administration (Figure 8A). Quantitative analysis of the fluorescence intensity in the hearts demonstrated that mice that received isoproterenol had no statistically significant increase in the fluorescence signal as compared with hearts from the mice that did not receive isoproterenol (Figures 8B and 8C). Previous investigations have demonstrated that a single bolus injection of 10 mg/kg isoproterenol produced myocardial necrosis and fibrosis in mdx mice as early as 8 h with a peak at ∼30 h and with evidence that the acute injury is resolved by 1 week.[41] Thus, in our study we analyzed the hearts 20 h after isoproterenol injection. Here there was no statistically significant difference between groups. Perhaps with future extensive additional experimentation, by varying isoproterenol dosing and time a significant protective effect could be obtained.

DISCUSSION

We show here, by using non-invasive optical imaging, the first direct evidence of the muscle membrane-interfacing intrinsic ability of synthetic copolymers to target damaged membranes at the muscle fiber, tissue, organ, and whole-animal levels *in vivo*. A far-red fluorescence probe was conjugated to the end group of P188 to enable high-fidelity tracking of synthetic copolymer-based membrane stabilizers in striated muscles *in vivo*. The main findings include direct optical evidence of the copolymer-muscle membrane interaction in cardiac and skeletal muscles, wherein the copolymer could be visualized interfacing with the sarcolemma but not entering the live muscle cell. Upon systemic copolymer delivery, results show a marked depot effect with long-term distribution and retention kinetics *in vivo*. In contrast, the Alx647 probe alone, by virtue of its inherent low membrane interaction factor,[29] did not interface with muscle membranes and had fast distribution and fast decay kinetics *in vivo*. Moreover, conjugation of Alx647 to P188 did not alter the membrane stabilization function of P188. Most importantly, findings show for the first time a significant muscle-disease-dependent homing and retention effect *in vivo*, with significantly greater P188-Alx647 fluorescence detected in skeletal muscles from dystrophin-deficient animals as compared with dystrophin-replete controls. These findings are discussed below in the context of therapeutic implications and insights on the molecular mechanism by which block copolymers interface with damaged muscle membranes.

The mechanism by which P188 preferentially localizes to dystrophic muscle membranes *in vivo* is not fully understood. Recent advances,

Average radiant efficiency area was measured to estimate the whole-body distribution of P188, with the same mice represented longitudinally and across different time points. The color bar indicates the total fluorescence radiant efficiency (photons s^{-1} cm^{-2} $steradian^{-1}$ per μW cm^{-2}). (C and D) Quantitative representation of the whole-body signal at the dorsal (C) and ventral (D) plane determined by region of interest (ROI) placement to capture the fluorescent signal. Results represent the average radiant fluorescence. P188-Alx647, dye-labeled copolymer; CTRL, control with no injection; Alx647, dye Alexa Fluor 647). Statistical significance was assessed by analysis of variance with the Tukey post test (*$p < 0.001$; #$p < 0.0001$). n = 4–7 per group. Hours 0–6 analysis: P188-Alx647 (n = 7); CTRL (n = 5); Alx647 (n = 4). Days 2–7 analysis: P188-Alx647 (n = 6); CTRL (n = 5); Alx647 (n = 4).

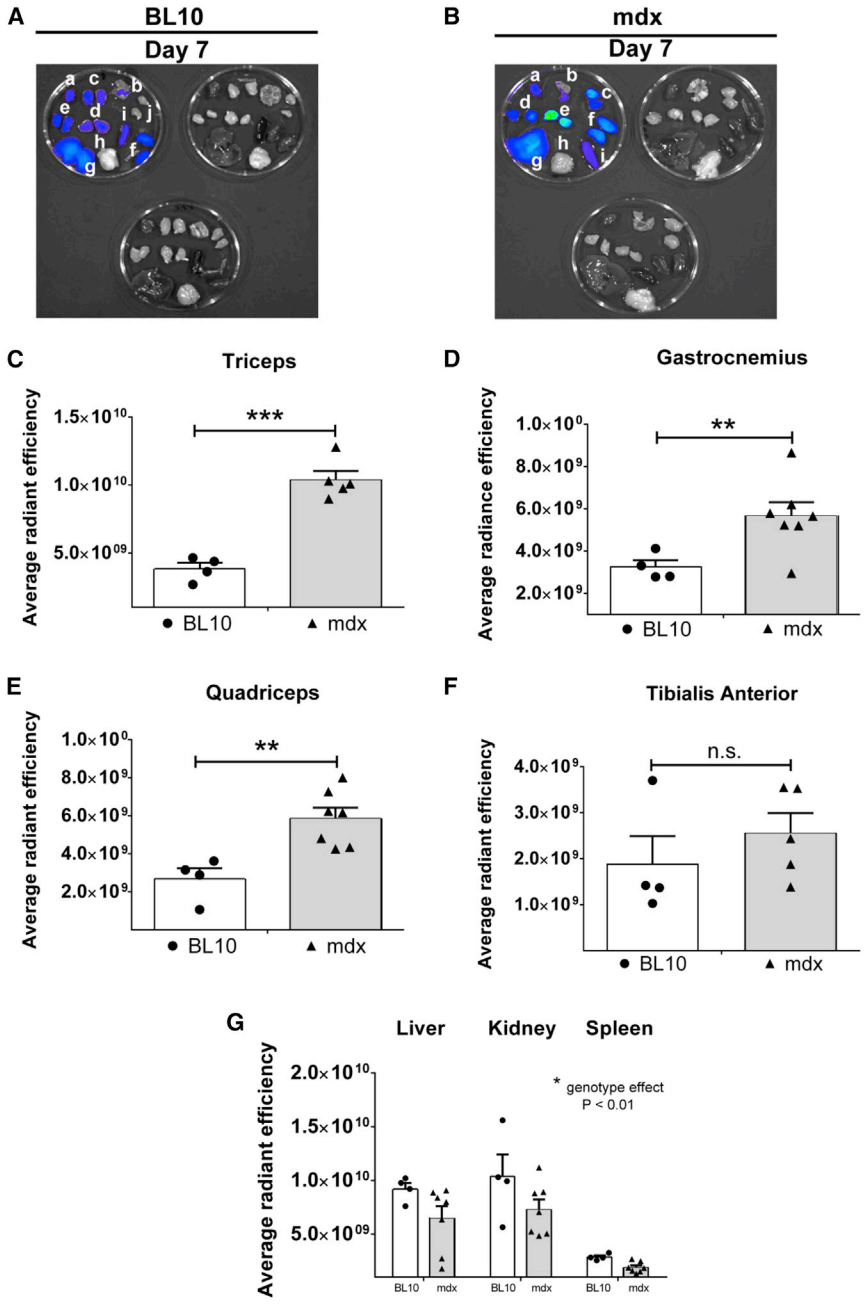

Figure 4. Greater *in vivo* retention of P188-Alx647 in dystrophic deficient skeletal muscles than in C57BL/10 controls

(A and B) *Ex vivo* imaging of excised tissues from BL10 (A) and mdx mice (B). a, heart; b, diaphragm; c, quadriceps; d, gastrocnemius; e, triceps; f, kidney; g, liver; h, brain; i, spleen. Top left Petri dish, P188-Alx647; top right Petri dish, Alx647; bottom Petri dish, CTRL. Images were acquired 7 days after single subcutaneous injection of P188-Alx647. The fluorescent images were acquired using the IVIS Spectrum instrument in epi-fluorescent mode (λ_{ex} = 650 nm, λ_{em} = 668 nm). The same color bar shown in Figure 3 was used in these analyses. (C–G) Quantification of fluorescence in the triceps (C), gastrocnemius (D), quadriceps (E), tibialis anterior (F), and excretory organs (G) from healthy (BL10) and dystrophin-deficient mice (mdx). *Ex vivo* tissue signals were determined by ROI placement to capture the fluorescent signal in each excised tissue. Results represent the average radiant efficiency fluorescence ± SE. Statistical significance was assessed by parametric tests unless indicated otherwise, followed by Welch's correction. Parametric tests were conducted for nearly all the analyses. In a few tests, owing to different Ns per group, normalcy tests could not be performed and thus a non-parametric test was conducted. Two-way ANOVA was used for analysis of non-muscle organs (main effects: organ and treatment). **p < 0.005; ***p < 0.0005, n = 4–7 per group. Day 7 mdx: P188-Alx647 (n = 7); CTRL (n = 5); Alx647 (n = 4). Day 7 BL10: P188-Alx647 (n = 4); CTRL (n = 4); Alx647 (n = 4).

these membrane structural alterations reveal a molecular substrate upon which copolymers, owing to physicochemical properties intrinsic to this class of chemistries, preferentially interface.

More specifically, we hypothesize, based on recent findings, that essential physicochemical properties of P188, encompassing architecture and hydrophilicity/hydrophobicity composition,[8,23,26,44] directly underlie the preferential targeting and retention of P188 to damaged muscle membranes *in vivo*. P188 has been shown to confer membrane protection against many different types of injuries, including DMD.[14,27,45–49] We and others have previously provided evidence that synthetic triblock copolymer P188 significantly protects dystrophic skeletal muscles during physiologically relevant mechanical stress *in vivo*.[23,25,44,48] Findings shown here provide the first direct evidence of copolymers surrounding individual muscle fibers upon systemic delivery *in vivo*, in direct support of the membrane stabilization mechanism of action of these molecular structures.[8] Biophysical studies examining triblock copolymer interactions with synthetic lipid membranes suggest that the hydrophobic PPO block plays a critical role in P188's interaction with the lipid

however, from molecular dynamics studies, together with cell and molecular copolymer-phospholipid membrane investigations, provide a foundation on which to propose the molecular basis for the *in vivo* findings reported here.[36] It is well known that the primary defect in DMD is loss of the dystrophin protein leading to severe muscle membrane instability.[1,2,8] Dystrophin deficiency causes marked alterations in phospholipid composition of the muscle membrane that, in turn, renders the membrane susceptible to injury as manifested by delta lesions in the membrane.[42,43] We hypothesize that

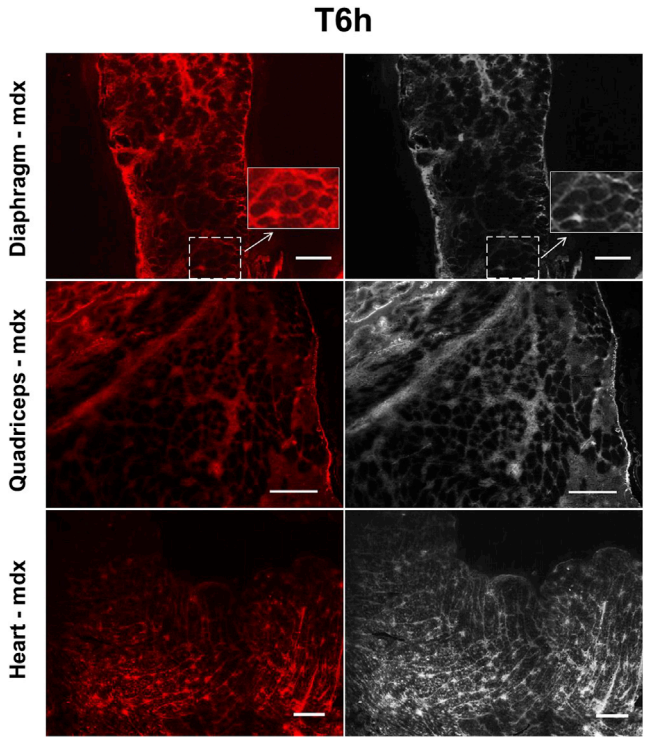

Figure 5. High-resolution confocal imaging shows direct evidence of P188 surrounding the sarcolemma of skeletal and cardiac muscle cells at 6 h following *in vivo* systemic delivery of P188-Alx647

Representative confocal microscopy with spectral detection and linear unmixing images were obtained from the diaphragm (top), quadriceps (middle), and heart (bottom) of mdx mice. The left panels show in red direct evidence of P188-Alx647 surrounding the sarcolemma of skeletal and cardiac muscle cells. The right panels show the same images in black-and-white with high contrast, evidencing the triblock copolymer P188 surrounding the cell membrane. Insets show magnifications of boxed regions, with skeletal muscle cell borders highlighted by P188-Alx647. Scale bars represent 200 μm for the quadriceps images and 100 μm for the diaphragm and heart images.

bilayer. Here, copolymer insertion is speculated to occur through the lipophilic portion of the molecule (PPO) adsorbing to the membrane surface and some penetration into the bilayer hydrocarbon core, with the hydrophilic tails (PEO) generally located in the adjacent water-rich layer.[39] The strength of this interaction appears to be highly dependent on the PPO/PEO mass ratio of the block copolymer, with hydrophobic dominant poloxamers (PPO/PEO mass ratio > 1) capable of inserting and subsequently permeabilizing the cell membrane.[50,51] In comparison, evidence is emerging that the relatively hydrophilic P188 (80% PEO) adsorbs onto the lipid membrane and exerts membrane stabilization by dampening surface and intra-bilayer hydration dynamics, rather than by direct corralling of lipids.[52] This dependence on the PPO/PEO mass ratio is supported by our group whereby we showed that an extended P188, a triblock copolymer featuring an equivalent PPO/PEO ratio to P188 but with a larger molecular weight, significantly stabilizes membranes *in vitro* and also *in vivo* in a manner dependent on both dosage and delivery route.[23]

Moreover, in the context of mechanistic investigation into the structure-function relationship of block copolymer architecture and chemistry, we recently showed that the addition of a single hydrophobic *tert*-butoxy end group to the PPO block in a PEO-PPO di-block significantly enhances membrane interaction and protection in dystrophic limb skeletal muscles during *in vivo* mechanical stress.[44] These findings suggest a marked biological effect of the hydrophobic PPO terminal end group on membrane stabilization *in vivo* and inform a novel "anchor and chain" model of copolymer-phospholipid membrane interaction whereby the addition of a hydrophobic end group "anchors" the PPO block within the alkyl tail region of the bilayer.[44] Recent all-atom *in silico* molecular dynamics studies provide further evidence that the intrinsic features of copolymer architecture and content serve as the driving elements by which these molecules interface and stabilize damaged membranes.[36] Taken together, we posit that these atomic and *in vitro* cellular-level findings translate to the whole animal to help account for the preferential homing/retention of P188 to DMD muscle observed here *in vivo*.

These findings, taken together with previous biophysical studies examining triblock copolymer interactions with lipid membranes,[39,50,51] along with a recent study demonstrating that poly(ethylene glycol)s are not retained in muscle tissues and are rapidly excreted via kidneys,[53] are evidence that elements of hydrophobicity and hydrophilicity underlie, at least partially, the preferential targeting and retention of P188 to damaged muscle membranes.

Synthetic block copolymers have numerous features that make them attractive as a potential therapy for DMD. First, the mechanism of action is not limited by the DMD-specific lesion. Thus, in principle, synthetic membrane stabilizers could be applicable to all DMD patients, regardless of genetic mutation. In addition, systemic distribution of block copolymers makes them ideal for treatment of all affected striated muscles in the body. Immunogenicity concerns of gene-based DMD treatments are also obviated by the use of synthetic sarcolemma stabilizers. One could envision initiating copolymer treatment soon after diagnosis, with the aim to preserve striated muscle function before marked muscle degeneration and wasting occurs. Membrane stabilizers may also be envisioned in bundled therapy. Block copolymers have been in use as vehicles for enhanced gene delivery in other applications,[54,55] and the prospect of bundled therapies of block copolymers and gene-directed strategies would be of significant interest to pursue in future works. Synthetic membrane stabilizers may ultimately extend to numerous other inherited or acquired diseases in which cell membrane integrity is compromised.

Placing these findings in clinical context, it is worth speculating that the rapid nature by which copolymers interface with and protect muscle membranes could have potential clinical benefits. For example, it is known that with rAAV-based gene addition there is comparatively slow onset kinetics, and fast-acting copolymers could provide a meaningful protective bridging mechanism while waiting for micro-dystrophin content to accrue to therapeutic levels in DMD muscles. This could make an interesting bundled therapy option to test in future

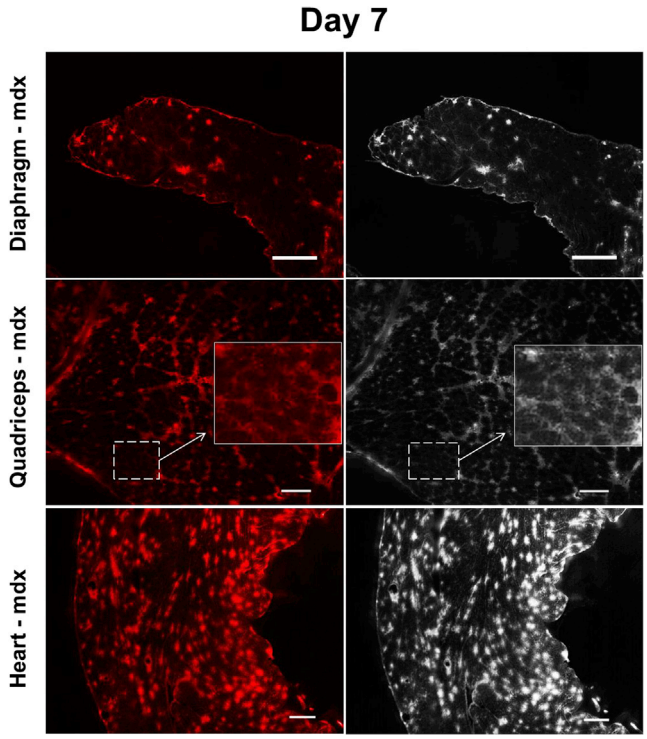

Figure 6. High-resolution confocal imaging shows direct evidence of P188 surrounding the sarcolemma of skeletal and cardiac muscle cells at day 7 following *in vivo* systemic delivery of P188-Alx647

Representative confocal microscopy with spectral detection and linear unmixing images were obtained from the diaphragm (top), quadriceps (middle), and heart (bottom) of mdx mice. The left panels show in red direct evidence of P188-Alx647 surrounding the sarcolemma of skeletal and cardiac muscle cells. The right panels show the same images as black-and-white with high contrast, evidencing the triblock copolymer P188 surrounding the cell membrane. Insets show magnifications of boxed regions, with skeletal muscle cell borders highlighted by P188-Alx647. Scale bars represent 200 μm for the quadriceps images and 100 μm for the diaphragm and heart images.

studies. There are potential limitations in implementing membrane stabilizers in the clinical arena, most notably, as our data show, that P188 steadily decays over time after systemic delivery *in vivo*. Because DMD is a chronic disease, membrane stabilizers would have to be delivered on a regular basis, similar in concept to clinical management in type I diabetic patients. In this regard it will be interesting and important to continue studies of membrane stabilizer mechanism of action with the goal of identifying chemistries with longer membrane interface dwell times that, in turn, could reduce dosing amounts and frequency of delivery. Because of the high cost of the Alx647 probe in this study, it is not practical to use this reagent in large animals. Nonetheless, it could be of interest in follow-up studies to more comprehensively examine the biodistribution of P188 in other valid DMD mouse models such as mdx/utr$^{+/-}$ and BL10 mdx mouse on a DBA2/J background (also termed D2-mdx or D2.B10-Dmdmdx/J; C57BL/10ScSn-Dmdmdx/J), shown to have marked muscular dystrophy. Furthermore, it is best for follow-up studies to perform further analysis of the route of injection, pending substantial additional financial support.

Extensive previously published studies on P188 distribution have centered on providing a comparative assessment of P188 pharmacokinetics across species that are commonly used in safety and efficacy evaluation studies.[27,28] These studies provide the central aspects of the P188 absorption, distribution, metabolism, and excretion (ADME) profile including elimination half-life, plasma clearance, plasma concentration, and urinary excretion among others. These data show that P188 is not metabolized in the body and is excreted via the kidneys. While these studies provide formative ADME background to the present work, they do not address the essential elements of the systemic distribution and discrete localization of P188 at the organ, tissue, and muscle fiber levels *in vivo*, as demonstrated herein.

In summary, by implementing high-resolution non-invasive optical imaging, this study provides the first direct evidence of copolymers surrounding the sarcolemma of skeletal and cardiac muscle cells *in vivo*, consistent with the membrane-stabilizing effects reported in cellular and molecular modeling studies. Imaging results demonstrate the increased localization and retention of synthetic membrane-interfacing copolymers to damaged muscle membranes in muscular dystrophy animals *in vivo*. Taken together, these findings provide direct evidence of muscle-disease-dependent molecular homing and retention of synthetic copolymers in striated muscles *in vivo*. These findings form the foundation on which to establish a physiologically comprehensive understanding of the intrinsic physicochemical features of block copolymers guiding muscle membrane association to confer protection *in vivo*.

MATERIALS AND METHODS

Study approval

All animal experiments were conducted in accordance with humane practices as directed by the Federal Animal Welfare Act, National Institutes of Health (NIH) guidelines, standards of the Association for Assessment and Accreditation of Laboratory Animal Care (AAALAC International), and at the university level under the regulation of the University Committee on the Use and Care of Animals. The protocols were approved by the University of Minnesota Institutional Animal Care and Use Committee.

Poloxamer 188 (Pluronic F68) was generously provided by BASF (Wyandotte, MI). *p*-Toluenesulfonyl chloride (>99%) was purchased from Acros Organics (Fair Lawn, NJ). Triethylamine (99%), tetrahydrofuran (HPLC grade), *N*,*N*-dimethylformamide (DMF) (certified ACS), and dichloromethane (certified ACS) were purchased from Fisher Scientific (Hampton, NH). Sodium azide (>99.5%), triphenylphosphine (99%), α-cyano-4-hydroxycinnamic acid (>98%), sodium trifluoroacetate (98%), and anhydrous *N*,*N*-dimethylformamide (99.8%) were purchased from Sigma-Aldrich (St. Louis, MO). Alx647 NHS Ester (*N*-hydroxysuccinimide ester) was purchased from Thermo Fisher Scientific (Waltham, MA). Molecular sieves (4 Å) were purchased from Mallinckrodt (Staines-upon-Thames,

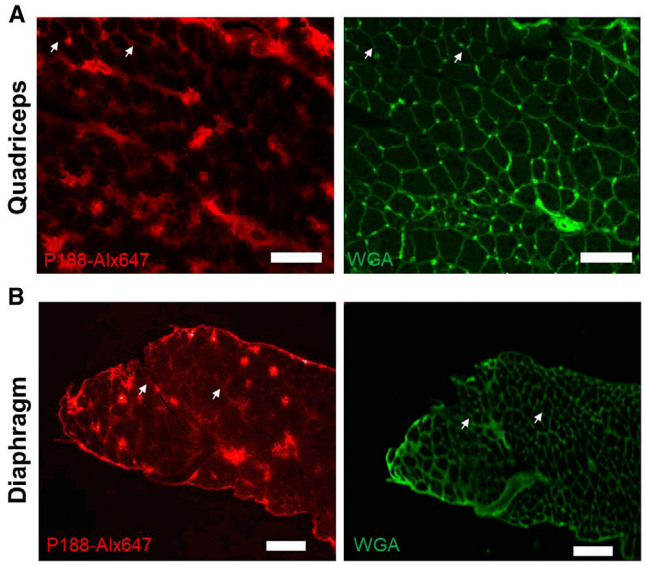

Figure 7. High-resolution confocal imaging shows direct evidence of P188 colocalizing with the membrane marker WGA

(A) Quadriceps and (B) Diaphragm from mdx mice injected with P188-Alx647 and stained with WGA at day 7. White arrows highlight the colocalization between P188-Alx647 and WGA at the sarcolemma. Scale bars represent 100 μm.

UK). PD-10 desalting columns were purchased from GE Healthcare (Chicago, IL).

Synthesis of Alx647-tagged P188

Alx647-tagged P188 (P188-Alx647) was prepared by end-group modification through four steps: (1) tosylation of the hydroxyl end group to synthesize tosyl-P188; (2) azide substitution of the tosyl group to yield N_3-P188; (3) amine reduction of the azide group to generate NH_2-P188; and (4) Alx647 conjugation to afford P188-Alx647 (Figure 1A).

Synthesis of tosyl-P188

P188 (10.4 g) was first dried by azeotropic distillation in toluene (∼120 mL). Fivefold molar excess of freeze-dried *p*-toluenesulfonyl chloride (1.18 g) and 25× molar excess of triethylamine (3.13 g) were rapidly added to the dried P188 in toluene under argon flow. The reaction mixture was stirred at room temperature overnight under a static argon atmosphere. After removing toluene by rotary evaporation, the crude product was dissolved in dichloromethane (DCM) and washed twice with water to remove excess triethylamine. After washing, the DCM layer was collected and condensed to ∼20 mL by rotary evaporation. The polymer dissolved in DCM was precipitated by dropwise addition into cold diethyl ether and then collected by vacuum filtration through a fine-frit glass Buchner funnel. The resulting tosyl-P88 was freeze-dried for subsequent azide substitution.

Synthesis of N_3-P188

DMF was dried over 4 Å molecular sieves. Dried DMF (∼60 mL) was transferred using a cannula to dissolve freeze-dried tosyl-P188 (2.18 g). 20× molar excess of sodium azide (0.38 g) was rapidly added to the polymer solution under argon flow. The reaction mixture was stirred overnight at 90°C under an argon atmosphere. After cooling down to room temperature, DMF was removed by rotary evaporation. The crude product was dissolved in DCM and washed twice with brine and twice with water. After washing, the DCM layer was collected and condensed to ∼20 mL by rotary evaporation. The polymer dissolved in DCM was precipitated by dropwise addition into cold diethyl ether and then collected by vacuum filtration through a fine-frit glass Buchner funnel.

Synthesis of NH_2-P188

N_3-P188 (0.85 g) and 15× molar excess of triphenylphosphine (0.44 g) were dissolved in ∼30 mL of tetrahydrofuran (THF). The reaction mixture was stirred at 40°C under reflux for 3 days, then ∼4 mL of water was added to the reaction mixture. After stirring for another 2 days THF was removed by rotary evaporation, and the crude product was dissolved in DCM. The polymer was precipitated by dropwise addition into cold diethyl ether and then collected by vacuum filtration through a fine-frit glass Buchner funnel. The resulting NH_2-P188 was freeze-dried in benzene. In this protocol, P188-azide was reduced by Staudinger reaction (to form the amine, using triphenylphosphine). By protocol optimization, the P188-azide was then reduced by hydrogenation instead of the Staudinger reaction, thus the amine was formed by hydrogenation of the azide using hydrogen gas and was catalyzed by palladium on carbon (Pd/C). This shortened the reaction time of this step to an overnight reaction with no observable chain coupling.

Synthesis of P188-Alx647

Anhydrous DMF was dried over 4 Å molecular sieves immediately before the reaction to fully dry the solvent. Dried DMF (∼2 mL) was cannula transferred to dissolve freeze-dried NH_2-P188 (52.8 mg). Triethylamine (20 drops) and Alx647 *N*-hydroxysuccinimide esters (10 mg) dissolved in anhydrous DMF were rapidly added to the polymer solution under argon flow. The reaction flask was wrapped with aluminum foil, and the reaction mixture was stirred at room temperature for 5 days. After removing DMF under vacuum, ∼2 mL of water was added to the crude product and the mixture was stirred for another 5 days to remove reactivity of excess Alx647 *N*-hydroxysuccinimide ester. The polymer was purified using a PD10 desalting column to remove residual triethylamine, DMF, and Alx647 dye. The resulting polymer was freeze-dried.

Molecular characterization

End-group modification was determined by peak analysis on the ^{1}H NMR and ^{13}C NMR spectra of polymers in deuterated water and deuterated chloroform, respectively. Spectra were obtained on a 400 MHz Bruker Avance IIIHD Nanobay AX-400 spectrometer. Molecular weight distributions of the polymers were determined with MALDI-TOF mass spectrometry (TOF 5800; Sciex, Washington, DC) using α-cyano-4-hydroxycinnamic acid as the matrix and sodium trifluoroacetate as a cationization agent.

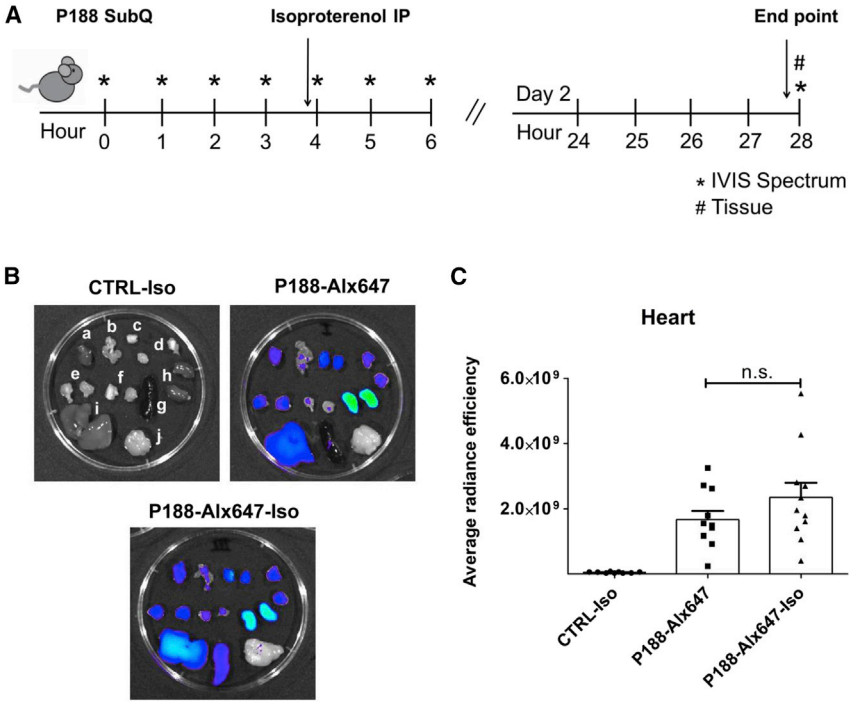

Figure 8. Detection of P188-Alx647 following acute cardiac stress in dystrophic heart *in vivo*

(A) Scheme outlining the design of acute isoproterenol-induced stress challenge. A single intraperitoneal injection of 10 mg/kg of isoproterenol (Iso) was given to young mdx male mice (P21–P25) 4 h after the administration of P188-Alx647. Asterisks denote the time points were the live images were acquired on the IVIS Spectrum. Hash mark denotes the endpoint for tissue collection and further analysis of P188-Alx647 distribution at the organ level. (B) *Ex vivo* imaging of excised tissues from mdx mice 28 h after P188-Alx647 administration and 24 h of Iso treatment. a, heart; b, diaphragm; c, tibialis anterior; d, triceps; e, gastrocnemius; f, quadriceps; g, spleen; h, kidney; i, liver; j, brain. The same color bar shown in Figure 3 was used in these analyses. (C) Quantification of fluorescence in the dystrophic heart 24 h after Iso treatment. *Ex vivo* tissue signals were determined by ROI placement to capture the fluorescent signal in the excised heart tissue. Results represent the average radiant efficiency fluorescence ± SEM, n = 9–11 per group. Statistical significance was assessed by unpaired t test with Welch's correction.

Hypo-osmotic stress and isotonic recovery assay, and enzyme release assay

The details of the assay can be found in Lu et al.[3] In brief, C2C12 myoblasts were incubated with 14 μM P188, 14 μM AlxP188, or 28 μM Alx647 in the following sequence: 330 mOsm isotonic buffer (140 mM NaCl, 5 mM KCl, 2.5 mM $CaCl_2$, 2 mM $MgCl_2$, and 10 mM HEPES, pH 7.2), 134 mOsm hypotonic buffer (composition equivalent to 330 mOsm solution but with NaCl reduced to 50 or 20 mM), then 330 mOsm isotonic buffer. Alx647 *N*-hydroxysuccinimide ester was incubated in water at 37°C for 7 days to remove *N*-hydroxysuccinimide ester before the cellular assay. The amount of LDH release in each step was measured using an LDH Assay kit (Pointe Scientific, Canton, MI) at 37°C. For this assay in general a total of six independent data points, as derived from individual wells, were conducted for each experiment. The LDH release at each step was normalized to the total amount of LDH per well. The fractional LDH release in the presence of the polymer was further normalized to the fractional LDH release without the polymer (non-treated).

Ventricular myocyte isolation and primary culture

Adult rat ventricular myocyte isolation was performed as previously described.[56] In brief, adult female rats (Sprague-Dawley—Envigo, strain #002) aged 3–4 months old were anesthetized by inhalation of isoflurane followed by intraperitoneal injection of heparin (15,000 U/kg) and pentobarbital sodium (Fatal Plus) (150 mg/kg). Following enzymatic digestion by retrograde perfusion with collagenase and gentle trituration of the cardiac ventricles, cardiac myocytes were plated on laminin-coated glass coverslips (2×10^4 myocytes/coverslip) and cultured in M199 medium (Sigma), supplemented with 25 mM HEPES, 26.2 mmol/L sodium bicarbonate, 0.02% BSA, and 50 U/mL penicillin-streptomycin, with pH adjusted to 7.4; additionally insulin (5 μg/mL), transferrin (5 μg/mL), and selenite (5 ng/mL) (ITS) were added (Sigma I1884). One hour after plating, non-adherent cells were removed and fresh M199 was applied.

In vitro P188 assays: Cardiac myocytes and flexor digitorum brevis

Cardiac myocytes were incubated in fresh M199 medium at a concentration of 2×10^4/mL for 24 h at 37°C and 5% CO_2 prior to the *in vitro* assays. Cardiac myocytes were incubated with 0.3 μM Calcein-AM for 10 min at 37°C in FluoroBrite Dulbecco's modified Eagle's medium (DMEM) (Gibco A1867901). After two gentle washes in FluoroBrite medium, cells were incubated in the same medium with 14 μM P188-Alx647 for 4 h at 37°C. Alx647 at 28 μM was used as a control for the experiment. After two washes the cardiomyocytes were kept in FluoroBrite DMEM and transferred to an incubator connected to the confocal microscope in the University of Minnesota imaging center (UMN UIC). Live cell images were taken using a Nikon A1R FLIM confocal microscope.

FDB fibers were isolated from C57BL/10J adult male mice (The Jackson Laboratory, strain #000665) by collagenase digestion and trituration. The fibers were plated on laminin-coated chambered coverslip in 300 μL of M199. After 30 min of stabilization at 37°C and 5% CO_2 incubator, FDB fibers were treated with 0.5 μM Calcein-AM (Invitrogen C3100) for 10 min at 37°C in FluoroBrite DMEM. After washing the coverslip with FluoroBrite DMEM twice, the FDB fibers were incubated with either 60 μM Alx647 and/or 30 μM P188-Alx647 for 4 h at 37°C. The coverslips were washed with FluoroBrite DMEM twice and transferred to an incubator connected to the confocal

microscope in the UMN UIC. Live cell images were taken using a Nikon A1R FLIM confocal microscope in the same way as for the cardiac myocytes.

In vivo study design

Mice were housed in cages, located in a well-ventilated, temperature-controlled room at 21°C ± 2°C with relative humidity ranging from 40% to 60% and a light/dark period of 12:12 h, with free access to water and food.

In vivo imaging

The IVIS Spectrum *in vivo* imaging system was used to dynamically assess the *in vivo* distribution of P188-Alx647. For the biodistribution study, mdx male mice (C57BL/10ScSn-*Dmd*^{mdx}/J, The Jackson Laboratory, strain #001801) and wild-type (WT) male mice (C57BL/10J) aged between postnatal day 21 (P21) and P25 (weighing between 8 and 11 g) were randomly separated into three groups: (1) P188-Alx647 treated; (2) Alx647 treated; and (3) no treatment. On day 1, dorsal and ventral fur was removed using a depilatory cream and a single subcutaneous injection of 150 mg/kg Alx647-labeled P188 copolymer diluted in saline (37 μM) corresponding to the maximal volume that can be administered subcutaneously (40 μL/g). Fluorescence of Alx647 dye was used as a control. Mdx and/or WT mice that did not receive any treatment were used as an additional control for background autofluorescence. Immediately after the fluorescence probe injection, anesthesia was induced with 2% isoflurane in 100% oxygen in the anesthetic chamber until loss of the righting reflex. Mice were then moved to the heated stage of the IVIS Spectrum and anesthesia was maintained using 1% isoflurane in 100% oxygen through an adapted nasal cone. Fluorescence imaging was performed, and mice were allowed to fully recover on a heating pad. Eye ointment was used to avoid dryness and to ensure animal wellbeing. For each imaging time point, the time from induction to recovery was estimated to be 10 min. Whole-length dynamic imaging was performed at T0, 1 h (T1 h), T2 h, T3 h, T4 h, T5 h, T6 h, day 2 (T24 h), day 3 (T48 h), day 4 (T72 h), day 5 (T96 h), day 6 (T120 h), and day 7 (T144 h) (Figure 3). Dorsal and ventral views were acquired constantly in the same field of view (C) using the IVIS Spectrum. After the final time point of each experiment (6 h or day 7 for the biodistribution study and day 2 for the isoproterenol study), the mice were euthanized using pentobarbital sodium overdose and the organs harvested for *in vivo* imaging (for details see the next section). For animal attrition, six mice, including two controls, two copolymer-injected mice, and two Alx647-injected mice, were excluded after cage flooding incidents to avoid confounding data analysis. These mice were excluded from the study at the time of the incident (day 2 and day 4), and no data were recorded after the incidents happened. In addition, two triceps and two TAs from the P188-Alx647-treated group had to be excluded from *ex vivo* analysis due to technical difficulties encountered with these mice during tissue harvest for fluorescence imaging. The IVIS Spectrum instrument is equipped with 10 narrow-band excitation filters and 18 narrow-band emission filters that assisted in significantly reducing autofluorescence. Imaging was performed on the IVIS Spectrum imaging system (PerkinElmer) by two-dimensional epifluorescence imaging with an excitation of 650 nm and emission of 668 nm at indicated times after P188-Alx647 injection. The spectrum system achieves superior spectral unmixing through a wide range of high-resolution, short-cutoff filters and advanced spectral unmixing algorithms. IVIS uses a back-thinned charge-coupled device cooled to −90°C to achieve maximum sensitivity. Although the IVIS has a high-sensitivity system measuring dark charge during down-time and running a self-calibration during initialization, we validated in each experiment that the system was working properly for our experiment. For this purpose, we tested for (1) potential tube-to-tube position variability on the platform, (2) machine variability, and (3) space variability by using the same concentration and volume of P188-Alx647 standards and rotating the plate to capture all possible sample positions. To confirm that the P188 concentration we were using was in the linear range of the system, a standard curve was used (0 μM, 3.1 μM, 6.2 μM, 12.5 μM, 18 μM, 25 μM, 37 μM, and 50 μM) and used for system calibration every time the mice were imaged. Data acquisition and processing were performed according to the Living Image v.4.3.1 protocol.

Ex vivo fluorescence assessment of tissues

For the *ex vivo* study, all animal experiments were performed in accordance with humane practices as called for by the Federal Animal Welfare Act, NIH guidelines, standards of AAALAC International, and at the university level under the regulation of the University Committee on the Use and Care of Animals. They were approved by the University of Minnesota Institutional Animal Care and Use Committee.

To determine the *in vivo* distribution/accumulation of P188-Alx647 on a more detailed level, each mouse tissues were harvested. Mice were euthanized at different times after P188-Alx647 or Alx647 injection (6 h and 7 days for the biodistribution study, 24 h for the isoproterenol study) using a pentobarbital sodium overdose (Fatal Plus). After transcardiac perfusion with 10 mL of PBS, the major organs including liver, spleen, kidneys, brain, heart, quadriceps, diaphragm, gastrocnemius, and triceps were collected. The isolated tissues were imaged and the fluorescence measured using the IVIS Spectrum imaging system. Images were taken in the far-red and NIR excitation and emission channels corresponding to the Alx647 spectrum using the epifluorescence mode of the IVIS Spectrum instrument. All quantitative measurements of fluorescence signal were performed using Living Image Analysis 4.7.3 software (PerkinElmer). After whole tissue imaging, hearts and skeletal muscles were processed for histological analysis as described below.

Image analysis

Data were analyzed using Living Image Analysis 4.7.3. For *in vivo* imaging, regions of interest (ROIs) were drawn in the defined area and quantified using the experimentally validated physical calibrated unit: "Radiant Efficiency [p/s/sr]/[μW/cm^2]."[57] To obtain the ROI values expressed in a calibrated, physical unit the Living Image software

normalizes automatically for sensitivity differences resulting from different exposure times, without the need for user input. For fluorescent imaging, the calibrated unit is "Radiant Efficiency." Fluorescence values are reported as "Average Radiant Efficiency" [p/s/cm^2/sr]/[μW/cm^2] (=Radiant Efficiency/ROI surface area), as detailed previously.[57] The ROIs were sized to encompass the entire fluorescent signal to ensure that the imaging data between individual animals/organs could be directly compared.

Isoproterenol acute stress challenge

Isoproterenol hydrochloride (Sigma #I6504) was dissolved in saline at a final concentration of 2 mg/mL and sterile filtered. The sterile isoproterenol solution was stored at 4°C for no more than 24 h and checked before use for any discoloration indicative of degradation. Isoproterenol was delivered 4 h after P188-Alx647 administration via intraperitoneal injections of 10 mg/kg in volumes adjusted for body weight.

Fluorescence imaging and spectral unmixing

Fresh excised hearts and skeletal muscles were cut in half along the transverse plane and placed into OCT medium to be frozen in liquid nitrogen-cooled isopentane and stored at −80°C. Seven-micrometer cryosections were obtained using the Leica cryostat at −20°C, and spectral imaging of the section was performed prior to any staining to preserve the tissue localization and prevent staining-related modification of the tissues-compound interaction. All staining was performed on unfixed tissue. The following reagents were used for immunofluorescence staining: goat serum for blocking (Jackson ImmunoResearch #005-000-121, 10%), WGA Alexa Fluor 488 conjugate (Thermo Fisher, 5 μg/mL), and ProLong Gold Antifade Mountant with DAPI (Thermo Fisher). After blocking, staining was performed as a single step at room temperature for 1 h, flanked by three 5-min washes in PBS. It is noteworthy that numerous fixation protocols, applied to whole muscle fixation and cryosection fixation, were used to preserve the compound tissue localization over the staining process; however, these were all unsuccessful, as they significantly altered the detection of the P188-Alx647 probe.

Nikon C2 upright spectral confocal imaging system

For the Nikon C2 upright spectral confocal imaging system, constant acquisition parameters in the spectral mode were set and used for all samples to obtain images suitable for quantification and comparison between samples. Pure P188-Alx647 and Alx647 spectra were acquired and used for spectral unmixing of the respective compounds in the images acquired to distinguish the specific compound signal from the background autofluorescence. Images were acquired using the Nikon C2 upright spectral confocal imaging system. Nikon Elements Imaging software (version 5.30.05) at the UMN UIC analysis station was used for the analysis of spectral unmixing and histology images.

Statistics

Statistical tests were calculated in GraphPad Prism, version 6.0 (GraphPad Software). An unpaired, two-tailed Student's t test was used to compare two groups unless indicated otherwise, followed by Welch's correction. One-way ANOVA was used to compare more than two groups with one independent variable, followed by Tukey's correction for multiple comparisons. Two-way ANOVA was used for analysis of non-muscle organs (main effects: organ and treatment). Parametric tests were conducted for nearly all the analyses. In a few tests, owing to different Ns per group, normalcy tests could not be performed and thus a non-parametric test was conducted, as detailed in the figure legends and Table S1.

DATA AVAILABILITY

All of the original data and materials presented here are available for distribution upon request.

SUPPLEMENTAL INFORMATION

Supplemental information can be found online at https://doi.org/10.1016/j.omtm.2022.12.005.

ACKNOWLEDGMENTS

This work was supported by grants from NIH (R01HL138490, R01HL132874, R01AR071349, and R01HL122323) and the Muscular Dystrophy Association. We are grateful to the assistance of the UMN UIC Nikon Center of Excellence Imaging group and members of the Metzger lab for helpful discussions.

AUTHOR CONTRIBUTIONS

A.B.B.A. conceived and designed the study, conducted animal experiments, analyzed data, and wrote the manuscript. H.C. helped design the study, conducted animal experiments, analyzed data, and wrote the manuscript. M.K. helped in designing the study, performed the P188-Alx647 synthesis and molecular characterization, analyzed data, and assisted in writing the manuscript. D.H. performed the FDB experiment and confocal images. N.V.Z. performed the P188-Alx647 synthesis and molecular characterization. T.P.L., M.A.H., B.J.H., and F.S.B. were essential in supervising M.K. and N.V.Z., and in conducting and editing the study. J.M.M. conceived and designed the study, supervised research, and aided in writing and editing the manuscript.

DECLARATION OF INTERESTS

J.M.M. is on the scientific advisory board and holds shares in Phrixus Pharmaceuticals Inc., a company developing novel therapeutics for heart failure. The terms of this arrangement have been reviewed and approved by the University of Minnesota in accordance with its conflict of interest policies.

REFERENCES

1. Flanigan, K.M. (2014). Duchenne and becker muscular dystrophies. Neurol. Clin. *32*, 671–688.
2. Sussman, M. (2002). Duchenne muscular dystrophy. J. Am. Acad. Orthop. Surg. *10*, 138–151.
3. Lu, Q.L., Rabinowitz, A., Chen, Y.C., Yokota, T., Yin, H., Alter, J., Jadoon, A., Bou-Gharios, G., and Partridge, T. (2005). Systemic delivery of antisense oligoribonucleotide restores dystrophin expression in body-wide skeletal muscles. Proc. Natl. Acad. Sci. USA *102*, 198–203.

4. Alter, J., Lou, F., Rabinowitz, A., Yin, H., Rosenfeld, J., Wilton, S.D., Partridge, T.A., and LU, Q.L. (2006). Systemic delivery of morpholino oligonucleotide restores dystrophin expression body wide and improves dystrophic pathology. Nat. Med. *12*, 175–177.

5. Malerba, A., Sharp, P.S., Graham, I.R., Arechavala-Gomeza, V., Foster, K., Muntoni, F., Wells, D.J., and Dickson, G. (2011). Chronic systemic therapy with low-dose morpholino oligomers ameliorates the pathology and normalizes locomotor behavior in mdx mice. Mol. Ther. *19*, 345–354.

6. Yokota, T., Lu, Q.L., Partridge, T., Kobayashi, M., Nakamura, A., Takeda, S., and Hoffman, E. (2009). Efficacy of systemic morpholino exon-skipping in Duchenne dystrophy dogs. Ann. Neurol. *65*, 667–676.

7. Mullard, A. (2021). Sarepta's DMD gene therapy falls flat. Nat. Rev. Drug Discov. *20*, 91.

8. Houang, E.M., Sham, Y.Y., Bates, F.S., and Metzger, J.M. (2018). Muscle membrane integrity in Duchenne muscular dystrophy: recent advances in copolymer-based muscle membrane stabilizers. Skelet. Muscle *8*, 31.

9. Bates, C.M., and Bates, F.S. (2017). 50th anniversary perspective: block polymers—pure potential. Macromolecules *50*, 3–22.

10. Padanilam, J.T., Bischof, J.C., LEE, R.C., Cravalho, E.G., TompkinS, R.G., Yarmush, M.L., and Toner, M. (1994). Effectiveness of poloxamer 188 in arresting calcein leakage from thermally damaged isolated skeletal muscle cells. Ann. N. Y. Acad. Sci. *720*, 111–123.

11. Adams-Graves, P., Kedar, A., Koshy, M., Steinberg, M., Veith, R., Ward, D., Crawford, R., Edwards, S., Bustrack, J., and Emanuele, M. (1997). RheothRx (poloxamer 188) injection for the acute painful episode of sickle cell disease: a pilot study. Blood *90*, 2041–2046.

12. Wang, T., Chen, X., Wang, Z., Zhang, M., Meng, H., Gao, Y., Luo, B., Tao, L., and Chen, Y. (2015). Poloxamer-188 can attenuate blood-brain barrier damage to exert neuroprotective effect in mice intracerebral hemorrhage model. J. Mol. Neurosci. *55*, 240–250.

13. Townsend, D., Turner, I., Yasuda, S., Martindale, J., Davis, J., Shillingford, M., Kornegay, J.N., and Metzger, J.M. (2010). Chronic administration of membrane sealant prevents severe cardiac injury and ventricular dilatation in dystrophic dogs. J. Clin. Invest. *120*, 1140–1150.

14. Markham, B.E., Kernodle, S., Nemzek, J., Wilkinson, J.E., and Sigler, R. (2015). Chronic dosing with membrane sealant poloxamer 188 NF improves respiratory dysfunction in dystrophic mdx and mdx/utrophin-/- mice. PLoS One *10*, e0134832.

15. Kim, M., Haman, K.J., Houang, E.M., Zhang, W., Yannopoulos, D., Metzger, J.M., Bates, F.S., and Hackel, B.J. (2017). PEO— PPO diblock copolymers protect myoblasts from hypo-osmotic stress in vitro dependent on copolymer size, composition, and architecture. Biomacromolecules *18*, 2090–2101.

16. Wong, S.W., Yao, Y., Hong, Y., Ma, Z., Kok, S.H.L., Sun, S., Cho, M., Lee, K.K.H., and Mak, A.F.T. (2017). Preventive effects of poloxamer 188 on muscle cell damage mechanics under oxidative stress. Ann. Biomed. Eng. *45*, 1083–1092.

17. Chang, D., Fox, R., Hicks, E., Ferguson, R., Chang, K., Osborne, D., Hu, W., and Velev, O.D. (2017). Investigation of interfacial properties of pure and mixed poloxamers for surfactant-mediated shear protection of mammalian cells. Colloids Surf. B Biointerfaces *156*, 358–365.

18. Collins, J.M., Despa, F., and Lee, R.C. (2007). Structural and functional recovery of electropermeabilized skeletal muscle in-vivo after treatment with surfactant poloxamer 188. Biochim. Biophys. Acta *1768*, 1238–1246.

19. Suzuki, N., Akiyama, T., Takahashi, T., Komuro, H., Warita, H., Tateyama, M., Itoyama, Y., and Aoki, M. (2012). Continuous administration of poloxamer 188 reduces overload-induced muscular atrophy in dysferlin-deficient SJL mice. Neurosci. Res. *72*, 181–186.

20. Borgens, R.B., Bohnert, D., Duerstock, B., Spomar, D., and Lee, R.C. (2004). Subcutaneous tri-block copolymer produces recovery from spinal cord injury. J. Neurosci. Res. *76*, 141–154.

21. Yasuda, S., Townsend, D., Michele, D.E., Favre, E.G., Day, S.M., and Metzger, J.M. (2005). Dystrophic heart failure blocked by membrane sealant poloxamer. Nature *436*, 1025–1029.

22. Martindale, J.J., and Metzger, J.M. (2014). Uncoupling of increased cellular oxidative stress and myocardial ischemia reperfusion injury by directed sarcolemma stabilization. J. Mol. Cell. Cardiol. *67*, 26–37.

23. Houang, E.M., Haman, K.J., Filareto, A., Perlingeiro, R.C., Bates, F.S., Lowe, D.A., and Metzger, J.M. (2015). Membrane-stabilizing copolymers confer marked protection to dystrophic skeletal muscle in vivo. Mol. Ther. Methods Clin. Dev. *2*, 15042.

24. Bartos, J.A., Matsuura, T.R., Sarraf, M., Youngquist, S.T., McKnite, S.H., Rees, J.N., Sloper, D.T., Bates, F.S., Segal, N., Debaty, G., et al. (2015). Bundled postconditioning therapies improve hemodynamics and neurologic recovery after 17 min of untreated cardiac arrest. Resuscitation *87*, 7–13.

25. Bartos, J.A., Matsuura, T.R., Tsangaris, A., Olson, M., McKnite, S.H., Rees, J.N., Haman, K., Shekar, K.C., Riess, M.L., Bates, F.S., et al. (2016). Intracoronary poloxamer 188 prevents reperfusion injury in a porcine model of ST-segment elevation myocardial infarction. JACC Basic Transl. Sci. *1*, 224–234.

26. Houang, E.M., Bartos, J., Hackel, B.J., Lodge, T.P., Yannopoulos, D., Bates, F.S., and Metzger, J.M. (2019). Cardiac muscle membrane stabilization in myocardial reperfusion injury. JACC. Basic Transl. Sci. *4*, 275–287.

27. Grindel, J.M., Jaworski, T., Emanuele, R.M., and Culbreth, P. (2002). Pharmacokinetics of a novel surface-active agent, purified poloxamer 188, in rat, rabbit, dog and man. Biopharm. Biopharm. Drug Dispos. *23*, 87–103.

28. Grindel, J.M., Jaworski, T., Piraner, O., Emanuele, R.M., and Balasubramanian, M. (2002). Distribution, metabolism, and excretion of a novel surface-active agent, purified poloxamer 188, in rats, dogs, and humans. J. Pharm. Sci. *91*, 1936–1947.

29. Hughes, L.D., Rawle, R.J., and Boxer, S.G. (2014). Choose your label wisely: water-soluble fluorophores often interact with lipid bilayers. PLoS One *9*, 87649.

30. Escobedo, J.O., Rusin, O., Lim, S., and Strongin, R.M. (2010). NIR dyes for bioimaging applications. Curr. Opin. Chem. Biol. *14*, 64–70.

31. Owens, E.A., Henary, M., El Fakhri, G., and Choi, H.S. (2016). Tissue-specific near-infrared fluorescence imaging. Acc. Chem. Res. *49*, 1731–1740.

32. Chen, Y., Li, L., Chen, W., Chen, H., and Yin, J. (2019). Near-infrared small molecular fluorescent dyes for photothermal therapy. Chin. Chem. Lett. *30*, 1353–1360.

33. Shaikh, S.R., Dumaual, A.C., Jenski, L.J., and Stillwell, W. (2001). Lipid phase separation in phospholipid bilayers and monolayers modeling the plasma membrane. Biochim. Biophys. Acta *1512*, 317–328.

34. Maskarinec, S.A., and Lee, K.Y.C. (2003). Comparative study of Poloxamer insertion into lipid monolayers. Langmuir *19*, 1809–1815.

35. Firestone, M.A., Wolf, A.C., and Seifert, S. (2003). Small-angle X-ray scattering study of the interaction of poly(ethylene oxide)-b-poly(propylene oxide)-b-poly(ethylene oxide) triblock copolymers with lipid bilayers. Biomacromolecules *4*, 1539–1549.

36. Houang, E.M., Bates, F.S., Sham, Y.Y., and Metzger, J.M. (2017). All-Atom Molecular Dynamics-Based Analysis of Membrane-Stabilizing Copolymer Interactions with Lipid Bilayers Probed under Constant Surface Tensions. The journal of physical chemistry. B *121*, 10657–10664.

37. McLennan, D.N., Porter, C.J.H., and Charman, S.A. (2005). Subcutaneous drug delivery and the role of the lymphatics. Drug Discov. Today Technol. *2*, 89–96.

38. Turner, P.V., Brabb, T., Pekow, C., and Vasbinder, M.A. (2011). Administration of substances to laboratory animals: routes of administration and factors to consider. J. Am. Assoc. Lab. Anim. Sci. *50*, 600–613.

39. Maskarinec, S.A., Hannig, J., Lee, R.C., and Lee, K.Y.C. (2002). Direct observation of poloxamer 188 insertion into lipid monolayers. Biophys. J. *82*, 1453–1459.

40. Yue, Y., Skimming, J.W., Liu, M., Strawn, T., and Duan, D. (2004). Full-length dystrophin expression in half of the heart cells ameliorates β-isoproterenol-induced cardiomyopathy in mdx mice. Hum. Mol. Genet. *13*, 1669–1675.

41. Meyers, T.A., Heitzman, J.A., Krebsbach, A.M., Aufdembrink, L.M., Hughes, R., Bartolomucci, A., and Townsend, D. (2019). Acute AT1R blockade prevents isoproterenol-induced injury in mdx hearts. J. Mol. Cell. Cardiol. *128*, 51–61.

42. Borgne, F.L., Guyot, S., Logerot, M., Beney, L., Gervais, P., and Demarquoy, J. (2012). Exploration of lipid metabolism in relation with plasma membrane properties of Duchenne muscular dystrophy cells: influence of L-carnitine. PLoS One *7*, 49346.

43. Mokri, B., and Engel, A.G. (1975). Duchenne dystrophy: electron microscopic findings pointing to a basic or early abnormality in the plasma membrane of the muscle fiber. Neurology *25*, 1111–1120.

44. Houang, E.M., Haman, K.J., Kim, M., Zhang, W., Lowe, D.A., Sham, Y.Y., et al. (2017). Chemical End Group Modified Diblock Copolymers Elucidate Anchor and Chain Mechanism of Membrane Stabilization. Molecular pharmaceutics *14*, 2333–2339.

45. Schaer, G.L., Spaccavento, L.J., Browne, K.F., Krueger, K.A., Krichbaum, D., Phelan, J.M., Fletcher, W.O., Grines, C.L., Edwards, S., Jolly, M.K., and Gibbons, R.J. (1996). Beneficial effects of RheothRx injection in patients receiving thrombolytic therapy for acute myocardial infarction. Results of a randomized, double-blind, placebo-controlled trial. Circulation *94*, 298–307.

46. Hannig, J., Zhang, D., Canaday, D.J., Beckett, M.A., Astumian, R.D., Weichselbaum, R.R., and Lee, R.C. (2000). Surfactant sealing of membranes permeabilized by ionizing radiation. Radiat. Res. *154*, 171–177.

47. Spurney, C.F., Guerron, A.D., Yu, Q., Sali, A., van der Meulen, J.H., Hoffman, E.P., and Nagaraju, K. (2011). Membrane sealant poloxamer P188 protects against isoproterenol induced cardiomyopathy in dystrophin deficient mice. BMC Cardiovasc. Disord. *11*, 20.

48. Lee, R.C., River, L.P., Pan, F.S., Ji, L., and Wollmann, R.L. (1992). Surfactant-induced sealing of electropermeabilized skeletal muscle membranes in vivo. Proc. Natl. Acad. Sci. USA *89*, 4524–4528.

49. Greenebaum, B., Blossfield, K., Hannig, J., Carrillo, C.S., Beckett, M.A., Weichselbaum, R.R., and Lee, R.C. (2004). Poloxamer 188 prevents acute necrosis of adult skeletal muscle cells following high-dose irradiation. Burns *30*, 539–547.

50. Wang, J.Y., Marks, J., and Lee, K.Y.C. (2012). Nature of interactions between PEO-PPO-PEO triblock copolymers and lipid membranes: (I) effect of polymer hydrophobicity on its ability to protect liposomes from peroxidation. Biomacromolecules *13*, 2616–2623.

51. Frey, S.L., Zhang, D., Carignano, M.A., Szleifer, I., and Lee, K.Y.C. (2007). Effects of block copolymer's architecture on its association with lipid membranes: experiments and simulations. J. Chem. Phys. *127*, 114904.

52. Cheng, C.Y., Wang, J.Y., Kausik, R., Lee, K.Y.C., and Han, S. (2012). Nature of interactions between PEO-PPO-PEO triblock copolymers and lipid membranes: (II) role of hydration dynamics revealed by dynamic nuclear polarization. Biomacromolecules *13*, 2624–2633.

53. Naito, M., Watanuki, Y., Toh, K., Yum, J., Kim, B.S., Taniwaki, K., Ogura, S., Ishida, H., Cho, M., Chaya, H., et al. (2022). Size-tunable PEG-grafted copolymers as a polymeric nanoruler for passive targeting muscle tissues. J. Control. Release *347*, 607–614.

54. Kabanov, A.V., Batrakova, E.V., and Alakhov, V.Y. (2002). Pluronic block copolymers as novel polymer therapeutics for drug and gene delivery. J. Control. Release *82*, 189–212.

55. Kabanov, A.V., Batrakova, E.V., and Miller, D.W. (2003). Pluronic block copolymers as modulators of drug efflux transporter activity in the blood-brain barrier. Adv. Drug Deliv. Rev. *55*, 151–164.

56. Thompson, B.R., Martindale, J., and Metzger, J.M. (2016). Sarcomere neutralization in inherited cardiomyopathy: small-molecule proof-of-concept to correct hyper-Ca2+−sensitive myofilaments. Am. J. Physiol. Heart Circ. Physiol. *311*, H36–H43.

57. Asem, H., Zhao, Y., Ye, F., Barrefelt, Å., Abedi-Valugerdi, M., El-Sayed, R., El-Serafi, I., Abu-Salah, K.M., Hamm, J., Muhammed, M., and Hassan, M. (2016). Biodistribution of biodegradable polymeric nano-carriers loaded with busulphan and designed for multimodal imaging. J. Nanobiotechnology *14*, 82.